INORGANIC CHEMISTRY FRONTIERS

CCS 中国化学会 CHINESE CHEMICAL SOCIETY

ROYAL SOCIETY OF CHEMISTRY

White light emission from co-doped La2Hf2O7 nanoparticles with suppressed host→Eu3+ energy transfer via U6+ co-dopant

Journal:	*Inorganic Chemistry Frontiers*
Manuscript ID	QI-RES-01-2021-000134.R1
Article Type:	Research Article
Date Submitted by the Author:	16-Apr-2021
Complete List of Authors:	Gupta, Santosh; Bhabha Atomic Research Centre, Radiochemistry Division Modak, Brindaban; Bhabha Atomic Research Centre, Chemistry Division, Chemistry Group Modak, Pampa; Atomic Energy Regulatory Board, Radiological Safety Division Mao, Yuanbing; Illinois Institute of Technology, Chemistry

White light emission from co-doped $La_2Hf_2O_7$ nanoparticles with suppressed host→Eu^{3+} energy transfer via U^{6+} co-dopant

Santosh K. Gupta[1,4*], Brindaban Modak[2,4], Pampa Modak[3,4], and Yuanbing Mao[5*]

[1]Radiochemistry Division, Bhabha Atomic Research Centre, Trombay, Mumbai-400085, India

[2]Chemistry Division, Bhabha Atomic Research Centre, Trombay, Mumbai-400085, India

[3]Radiological Safety Division, Atomic Energy Regulatory Board, Anushaktinagar, Mumbai 400094, India

[4]Homi Bhabha National Institute, Anushaktinagar, Mumbai – 400094, India

[5]Department of Chemistry, Illinois Institute of Technology, 3101 South Dearborn Street, Chicago, IL 60616, USA

*To whom correspondence should be addressed. Electronic mail: santoshg@barc.gov.in or santufrnd@gmail.com (SKG) and ymao17@iit.edu (YM). Tel.: +91-22-25590636 (SKG) and +1-312-567-3815 (YM).

Abstract

Controlled energy transfer has found to be one of the most effective ways of designing tunable and white photoluminescent phosphors. Utilizing host emission to achieve the same would lead to a new dimension in design strategy for novel luminescent materials in solid state lighting and display devices. In this work, we have achieved controlled energy transfer by suppressing host to dopant energy transfer in $La_2Hf_2O_7$:Eu^{3+} nanoparticles (NPs) by co-doping with uranium ion. Uranium acts as a barrier between oxygen vacancies of the $La_2Hf_2O_7$ host and Eu^{3+} doping ion to increase their separation and reduce the non-radiative energy transfer between them. Density functional theory (DFT) calculation of cohesive energy showed that Eu^{3+} dopant occupies La^{3+} site and uranium ion occupies Hf^{4+} site. Co-doping the $La_2Hf_2O_7$:Eu^{3+} NPs with uranium ions also creates negatively charged lanthanum and hafnium vacancies making the system highly electron rich. Formation of cation vacancy is expected to compensate the excess charge in the U and Eu co-doped $La_2Hf_2O_7$ NPs suppressing the formation of oxygen vacancy. This work shows how one can utilize the full color gamut in the $La_2Hf_2O_7$:Eu^{3+},U^{6+} NPs with the blue, green and red emissions from the host, uranium and europium, respectively, to produce near perfect white light emission.

Keywords: $La_2Hf_2O_7$; Europium; Uranium; Nanoparticles; Energy transfer; White light

1. Introduction

Phosphor converted light emitting diodes (pc-LEDs) is considered one of the most extraordinary invention in modern day owing to its extremely beneficial properties such low power consumption, high energy output, high brightness, environmental friendliness, etc.[1,2] To generate white light, some methods require mixing of red, green and blue light emitting phosphors or suitable dopant ions in a single host.[3,4] $La_2Hf_2O_7$ (LHO) has all the desirable credentials as a photoluminescence (PL) host owing to its low defect density, moderate phonon energy, optimum band gap, high thermal and structural stability, structural flexibility, radiation tolerance and ability to accommodate large concentration of dopant ion at both A and B sites.[3,5,6] There have been reports including ours wherein LHO doped with various lanthanide ions (Ce^{3+}, Pr^{3+}, Sm^{3+}, Eu^{3+}, Tb^{3+}, Dy^{3+}, etc.) has been explored for visible photoluminescence and radioluminescence.[3,6,7,8,9,10,11,12,13,14,15] In the above mentioned literature, Pr^{3+}/Eu^{3+} doping is used for generate red emission, Sm^{3+} for orange, Tb^{3+} for green, Pr^{3+},Ti^{4+} for persistent luminescence, and Dy^{3+} for yellow/blue, etc. These ions create certain strains in the host lattice and could induce severe structural distortion to hamper color efficiency of white light phosphors.[16] Role of luminescent hosts is found to be the key for optically active ions in relaxing forbidden f-f transition of lanthanide ions.[17,18] For most phosphors, the intrinsic emission of hosts due to charge transfer or defects is lost as most of the photoluminescence (PL) in those materials is triggered by host to dopant energy transfer (HDET).[19,20,21] Matching of energy states between luminescent hosts and dopant ions plays an important role in harvesting light emission zone of LEDs.[22,23,24,25] There is no report on restricting host-dopant energy transfer to utilize the emissions of hosts and dopant ions. Singh *et al.* reduced the energy transfer efficacy of vanadate (VO_4^{3-}) to lanthanide ion of YVO_4:Ln^{3+} by phosphorus co-doping.[26] Being a *p*-block element and of much smaller in size compared to 4f-block lanthanide ion, phosphorus encapsulation in the YVO_4 lattice leads to an unstable, strained and distorted phosphor.[27,28] Chung *et al.* used blocking unit such as 2-phenylpropan-2-yl to suppress the HDET in organic phosphors.[29] There has been a report on judiciously controlling HDET of $VO_4^{3-} \rightarrow Eu^{3+}$ by optimizing the dopant concentration in YVO_4:Eu^{3+}.[30]

In general, when a lanthanide ion is selected as the co-dopant, it suffers from poor absorption coefficient. On the other hand, transition metal ion is unlikely to have a large overlap of emission spectrum with the excitation spectrum of Eu. It was reported that uranium (UO_6^{6-}) and Eu^{3+} co-

exist in cubic lattice easily with reported energy transfer of 5f uranium ion to 4f Eu^{3+} in $ZnAl_2O_4$.[31] We are yet to find a report wherein defect emission is controlled by 5f ions to utilize the full electromagnetic spectrum.

Based on our recently studies on $A_2M_2O_7$ pyrochlore nanoparticles (NPs),[3,5,6] here we have co-doped 4f Eu^{3+} ion and 5f U^{6+} ion with much closer size match inside luminescence $La_2Hf_2O_7$ (LHO) host with controlled HDET. We judiciously utilized the emission of violet-blue (defect induced host emission), red (europium ion emission) and green PL (octahedral uranate emission) from LHO, LHO:Eu^{3+} (LHOE), and LHO:U^{6+} (LHOU) NPs, respectively, under UV irradiation to generate white light. Specifically, this work was taken up to simultaneously utilize all three emission bands coming from LHO host defect, europium and uranium to generate tunable emission and white color under single excitation wavelength while using Eu^{3+} as a dopant ion and U^{6+} as co-dopant. Furthermore, theoretical modeling was carried out using density functional theory (DFT) to predict the local site of dopant and co-dopant and probe chemical insight into the role of uranium dopant in quenching host to dopant energy transfer. This work offers a new strategy in utilization of doped pyrochlore NPs for multicolor emission and a new way to inhibit HDET.

2. Experimental

The materials used in the synthesis are lanthanum nitrate hexahydrate ($La(NO_3)_3 \cdot 6H_2O$, 99.0%), hafnium dichloride oxide octahydrate ($HfOCl_2 \cdot 8H_2O$, 98%), europium(III) nitrate pentahydrate ($Eu(NO_3)_3 \cdot 5H_2O$, 99.9%), and uranyl nitrate hexahydrate ($UO_2(NO_3)_2 \cdot 6H_2O$, 98-102%). LHO, LHOE (Eu^{3+} = 1.0%), LHOU (U^{6+} = 1.0%), and LHOEU (Eu^{3+} = 1.0% and U^{6+} = 0.1, 0.25, 0.5, 0.75, 1.0, 1.5, and 2.0%) NPs were synthesized using a molten salt synthesis (MSS) method employing the $NaNO_3$-KNO_3 mixture as a molten salt at 650°C.[5,6] The details of the synthesis process are well explained in the above-mentioned references. Specifically, stochiometric amount of starting reactants were used with the LHOEU NPs as an example. First, 5(1-x-y) mmol of $La(NO_3)_3 \cdot 6H_2O$, 5 mmol $HfOCl_2 \bullet 8H_2O$, 5x mmol $Eu(NO_3)_3 \cdot 5H_2O$, and 5y mmol $UO_2(NO_3)_2 \cdot 6H_2O$ were weighted and dissolved in 200 mL of deionized water (18.2 MΩ at 25°C). The aqueous solution of the starting reactants was mixed for 30 minutes using a magnetic stirring bar. Then, the solution was titrated with 200 mL of 10% ammonium hydroxide solution (NH_4OH, 28-30%) in a time range of 2 hours. A cloudy precipitate formed at the bottom of the beaker. The precipitate was collected through vacuum filtration, washed till pH value of the filtrate solution

was neutral, and then dried overnight in air at room temperature. This resulted in a final single-source complex precursor (1-x-y)$La(OH)_3$·x$Eu(OH)_3$·y$U(OH)_3$·$HfO(OH)_2$·nH_2O. In the second step, the LHOEU NPs were synthesized through a facile molten salt synthetic process using this single-source complex precursors and nitrate mixture ($NaNO_3$:KNO_3 = 1:1, molar ratio) at 650℃ for 6 hours. The empirical equations which govern the synthesis of the LHOEU NPs would be:

5(1-x-y) mmol $La(NO_3)_3·6H_2O$ + 5 mmol $HfOCl_2·8H_2O$ + 5x mmol $Eu(NO_3)_3·5H_2O$ + 5y mmol $UO_2(NO_3)_2·6H_2O$ → (1-x-y)$La(OH)_3$·x$Eu(OH)_3$·y$U(OH)_3$·$HfO(OH)_2$·nH_2O → [(1-x-y)La·xEu·yU]$_2Hf_2O_7$.

Caution: ^{238}U (depleted uranium) is a weak α-emitting radionuclide with a half-life of 4.47×10^9 years. To avoid health risks, it should be handled carefully by trained personnel with all possible personal protective equipment (PPE) in a good quality lab equipped with glove box and fume hood.

X-ray diffraction (XRD) was carried out using BRUKER™ D8 X-ray Diffractometer with a Cu $K_{\alpha 1}$ radiation (λ = 0.15406 nm, 40 kV, 40 mA) by a 2θ scanning mode ranging from 10° to 90° and a scanning step size of 0.04° at a scanning rate of 2.0° min^{-1}. Raman spectra were elucidated using a Renishaw 2000 Micro-Raman spectroscopy equipped with an argon laser (514.5 nm) in the range of 200–1000 cm^{-1}. The microstructure and morphology of the NPs were studied using a Carl Zeiss sigma VP scanning electron microscopy (SEM) equipped with a field emission gun operated at 5 kV. TEM images were recorded using Hitachi HF 3300TEM/STEM. PL emission and excitation spectroscopy were investigated using an Edinburgh Instruments FLS980 fluorometer system equipped with a steady state xenon source.

The first-principles calculations was performed using Vienna ab initio simulation package (VASP).[32,33] We performed electronic structure calculations for $La_2Hf_2O_7$ in the presence and absence of dopant elements. The projector augmented wave (PAW) pseudo potentials were used for the ion-electron interactions including the valence states of La ($5p^6 5d^1 6s^2$,9 valence electrons), Hf ($5d^3 6s^1$,4 valence electrons), O ($2s^2 2p^4$, 6 valence electrons), Eu ($5p^6 5d^1 6s^2$, 9 valence electrons), U ($5f^2 6s^2 6p^6 6d^2 7s^2$,14 valence electrons). The generalized gradient approximations (GGA) of Perdew−Burke−Ernzerhof (PBE) were used during the structure optimization procedure.[34,35] The plane wave basis with kinetic energy cut off of 500 eV and energy convergence of 10^{-6}eV for self-consistent iteration have been chosen. Brillouin zone sampling has been performed by Γ-centered k-point mesh of 6 ×6 × 6 using Monkhorst and Pack scheme. For

all the model structures, the relaxation of both cell parameter and ionic positions during geometry optimization has been taken into account.[36] The calculation of density of states (DOS) were performed using Γ-centered k-point mesh of 7 ×7 × 7.

3. Results and Discussion

3.1. X-ray diffraction (XRD)

Figure 1a shows the XRD patterns of the LHO, LHOE (Eu^{3+} = 1.0%), LHOU (U^{6+} = 1.0%) and LHOEU (Eu^{3+} = 1.0% and U^{6+} = 1.0%) NPs. The XRD patterns show eight major identifiable diffraction peaks with (hkl) values of (222), (400), (440), (622), (444), (800), (662), and (840). They all are well in agreement with the reported XRD pattern of undoped and doped $La_2Hf_2O_7$.[3] It is clearly seen that neither U/Eu doping nor Eu and U co-doping distorted the basic $La_2Hf_2O_7$ pyrochlore structure. The calculated crystallite size using the Debye-Scherer equation and lattice parameter of all above mentioned four samples are mentioned in Table 1. The calculated crystallite sizes are not affected much and are in the range of 27.4-28.8 nm for all the samples.

The lattice parameter did show some variations compared to the undoped LHO NPs (10.83 Å) with reduction for both LHOE (10.77 Å) and LHOU NPs (10.68 Å) whereas the LHOEU NPs assumed the value of 10.71Å. This is expected due to the smaller ionic radius of both Eu^{3+} (1.07 Å) and U^{6+} (0.86 Å) compared to La^{3+} (1.16 Å) in 8-coordination.

However, it should be noted that XRD sometimes fail to sense the presence of weak pyrochlore reflections, which should be confirmed with further structural analysis by other techniques such as Raman spectroscopy.

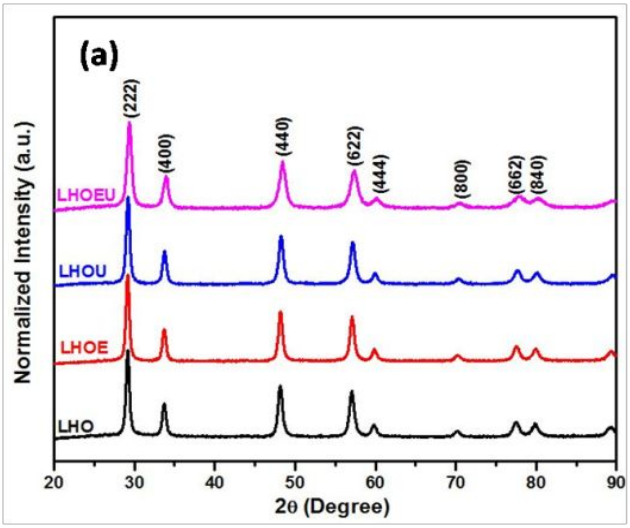

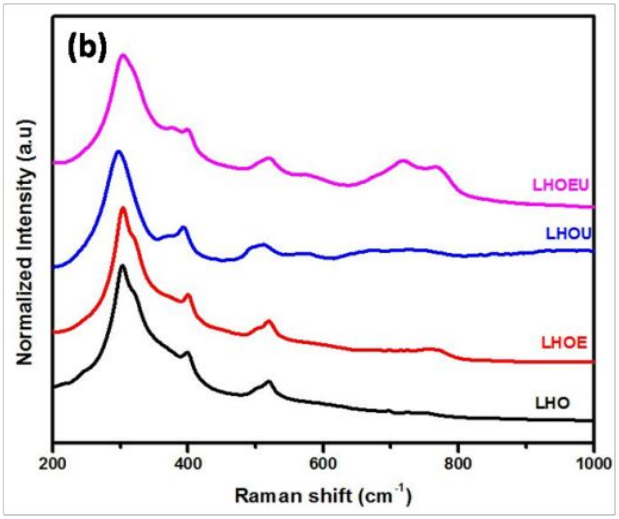

Figure 1. (a) XRD patterns and (b) Raman spectra of the LHO, LHOE, LHOU, and LHOEU NPs.

Table 1. Calculated crystallite size and lattice parameter of the LHO, LHOE, LHOU, and LHOEU NPs.

NPs	Crystallite size (nm)	Lattice parameter (Å)
LHO	27.4 ± 0.5	10.83
LHOE	28.8 ± 0.5	10.77
LHOU	27.7 ± 0.5	10.68
LHOEU	28.7 ± 0.5	10.71

3.2. Raman Spectroscopy

Radius ratio (r_A/r_B) plays an important role in deciding the exact structure of $A_2B_2O_7$ compounds. When $r_A/r_B > 1.46$, an order pyrochlore of $A_2B_2O_7$ compounds is the most prevalent structure.[37] Based on the concepts of group theory, the Raman spectra of ideal pyrochlore $A_2B_2O_7$ compounds ($Fd\bar{3}m$ space group) consist of six well-defined sharp vibrational peaks in the range 200-1000 cm^{-1}, which are ascribed to $A_{1g} + E_g + 4F_{2g}$.[38,39] LHO prefers to stabilize in ideal pyrochlore structure due to r_{La} (CN = 8) = 1.16 Å and r_{Hf} (CN = 6) = 0.710 Å giving a radius ratio value r_{La}/r_{Hf} = 1.63. Figure 1bshows the Raman spectra of the LHO, LHOE, LHOU, and LHOEU NPs. All of them exhibited peaks located approximately at 306, 320, 397, 498, 519, and 615 cm^{-1} which correspond to F_{2g}, E_g, F_{2g}, A_{1g}, F_{2g}, and F_{2g} modes, respectively.[40] Specifically, the peaks at 306,320, and 397 cm^{-1} are originated from the vibrations of the metal–oxygen bonds (in this case, La–O and Hf–O bonds, respectively). The peaks at 519 cm^{-1} and 615 cm^{-1}arise from the Hf–O stretching whereas the 498 cm^{-1} peak arising from the A_{1g} mode ascribed to the bending of Hf-O bond in HfO_6 octahedra.[41] The small peak around 769 cm^{-1} is ascribed to the distortion of the HfO_6 octahedra.[42] Therefore, based on our Raman data, all four of these samples showed the ideal pyrochlore structure. Moreover, the 769 cm^{-1} intensified along the order of LHO, LHOU, LHOE, and LHOEU NPs, which suggested doping of Eu^{3+} and U^{6+}, especially their co-doping, led to increased distortion of HfO_6 octahedra.

3.3. Geometry and electronic structure of LHO

$La_2Hf_2O_7$ crystallizes in the cubic perovskite structure, in which La sits on the polyhedral LaO_8, coordinated to eight oxygen, and Hf sits on the polyhedral HfO_6, coordinated to six oxygen (Figure 2a). Our calculated value of equilibrium lattice parameters using PBE functional is 10.83Å (volume = 1270Å^3) which is in good agreement with the experimental value of 10.776 Å.[43] Figure 2b shows the calculated DOS and PDOS of pure $La_2Hf_2O_7$. It is evident that the valence band maxima (VBM) are mainly composed of O 2p states. The bottom part of the conduction band (CB) mainly originates from La 4f states with minor contribution of La 5d and Hf 5d states. Our calculated band gap is 4.30 eV, which is close to the earlier DFT calculated value of 4.18 eV,[9] but it is lower than the experimental value of 5.6 eV.[44]

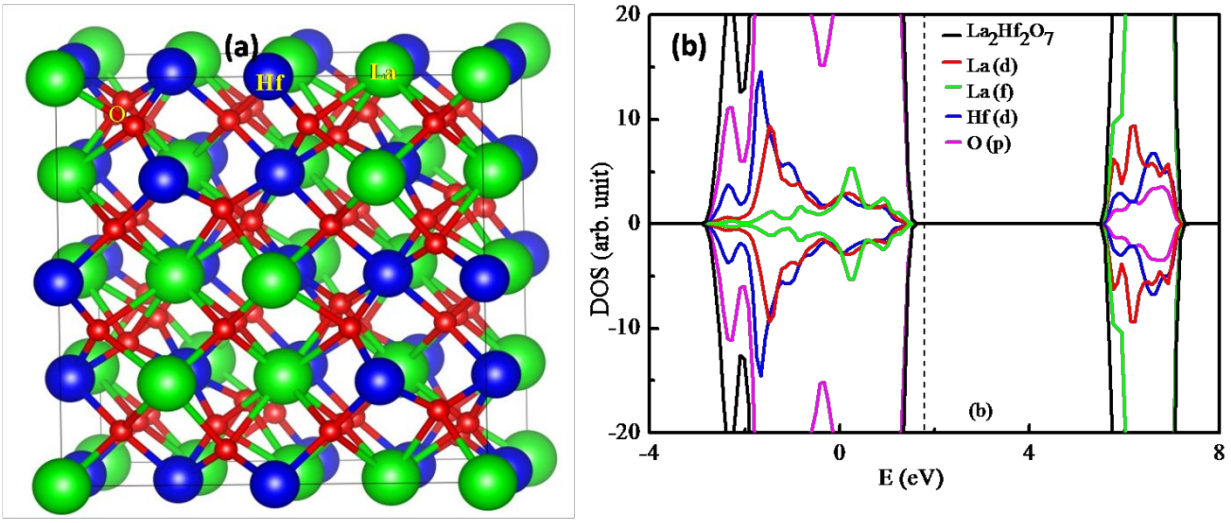

Figure 2. Calculated (a) crystal structure and (b) density of states of $La_2Hf_2O_7$. Vertical dashed line in (b) indicates the Fermi level.

3.4. Morphological Study: SEM and TEM

Figures 3a-d shows the SEM images of the LHO, LHOE, LHOU, and LHOEU NPs, respectively. The SEM micrographs show the formation of nanosized ellipsoids with an average diameter (corresponding size distribution histograms shown in Figure S1) in close agreement with the calculated crystallite size using the Debye-Scherer equation from the XRD data (Figure 1a). All SEM images clearly showed that the as-synthesized particles are in nanosized domain and spherical in shape. However, there is certain degree of agglomeration in all these samples. High surface area to volume ratio of NPs provides a very high surface energy. To minimize the surface energy, NPs tend to agglomerate, especially during the drying process after cast-dropping their dispersion on the SEM

sample holder. Agglomeration of NPs may occur due to attractive van der Waals forces between them. The morphology of these NPs remain the same with well-defined grain boundaries even with Eu or U doping and Eu,U co-doping into the LHO host showing the capability of our synthesis procedure. Representative TEM images of the LHO and LHOU NPs (Figures 3e and 3f, respectively) clearly show the formation of slightly agglomerated ellipsoidal NPs.

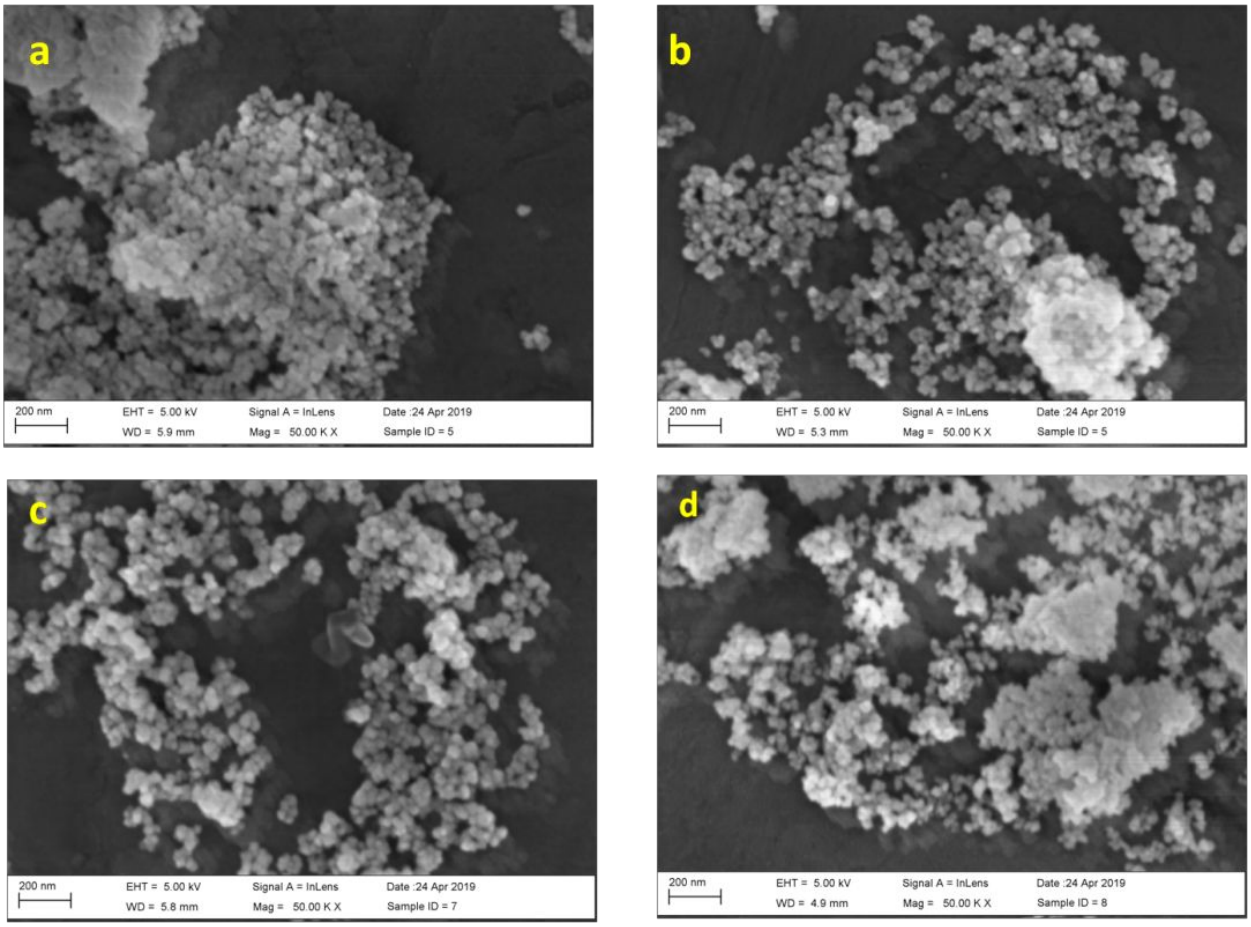

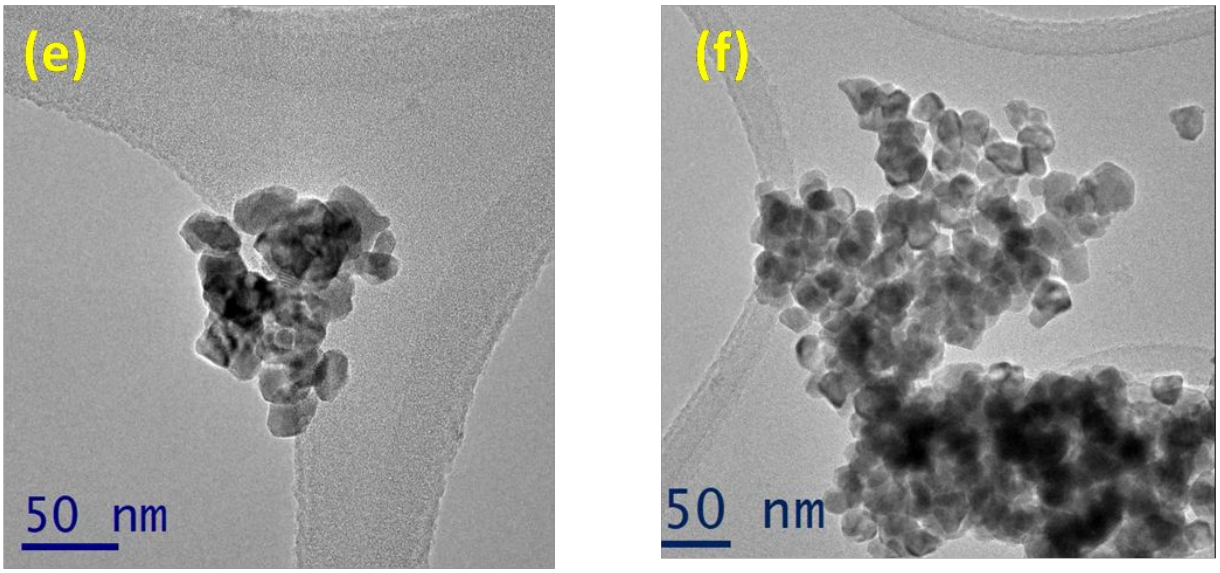

Figure 3. SEM images of the (a) LHO, (b) LHOE, (c) LHOU, and (d) LHOEU NPs. Representative TEM images of the (e) LHO and (f) LHOU NPs.

3.5. DFT calculated defect formation energies

In the present study, we have considered 88 atoms cell of the LHO host for the construction of the doped systems. For Eu doping, we have considered two scenarios, substitution of one La by Eu (Eu_{La}) and substitution of one Hf by Eu (Eu_{Hf}). Similarly, for U doping into $La_2Hf_2O_7$, we have considered two scenarios, substitution at the La lattice site (U_{La}) and substitution at the Hf lattice site (U_{Hf}). Similarly, for (Eu,U)-co-doped $La_2Hf_2O_7$, we have considered four different possibilities:(1) doping of both Eu and U at the La lattice sites ($Eu_{La} + U_{La}$), (2) doping of both Eu and U at the Hf lattice sites ($Eu_{Hf} + U_{Hf}$), (3) doping of Eu at the La lattice site while U at the Hf lattice site ($Eu_{La} + U_{Hf}$), and (4) doping of Eu at the Hf lattice site while U at the La lattice site ($U_{La} + Eu_{Hf}$). In each case, we have considered two different geometries by varying the relative distance between the two dopant elements. For the first case, we have chosen nearest neighboring lattice sites while they are far away from each other for the second case. Comparison of the energy of the optimized geometries for the model structures indicates that both the structures are energetically very close to each other (energy difference range = 0.002 – 0.05 eV).To find out preferred lattice site of the LHO host for Eu and U doping, the defect formation energies of different configurations have been computed using the relationship below:[45,46]

$$\Delta H_f = E_{defect} - E_{perfect} + q\sum n_x \mu_x \quad (1)$$

where E_{defect} and $E_{perfect}$ represent the energy of the doped and perfect $La_2Hf_2O_7$ calculated with the same supercell size, μ_x indicates the chemical potential of the element X, and n_x is the number of elements added (q = -1) or replaced (q = +1) to form the defect system. The formation energy for doping of Eu at La site is lower by 3.44 eV in comparison to that of Eu doping at Hf site. This indicates preferential occupation of Eu atoms at the lanthanum (La^{3+}) site over hafnium (Hf^{4+}) site. Therefore, the calculated defect formation energy of the Eu-doped $La_2Hf_2O_7$ system reveals that the probability of formation of Eu_{La} defect is more favorable in comparison to that of Eu_{Hf}. In contrast to Eu, uranium shows more preference for Hf lattice site over La site. The calculated formation energy for U_{Hf} is found to be lower by 0.56 eV with respect to that of U_{La}. On the other hand, for Eu and U co-doped $La_2Hf_2O_7$, the calculated defect formation energy follows the order (Eu_{La} + U_{Hf})-$La_2Hf_2O_7$ (0.82 eV) < (Eu_{Hf} + U_{Hf})-$La_2Hf_2O_7$ (0.90 eV) < (U_{La} + Eu_{Hf})-$La_2Hf_2O_7$ (1.45eV) < (Eu_{La} + U_{La})-$La_2Hf_2O_7$ (1.84eV). Thus, based on the formation energy calculation it can be concluded that the co-doping with Eu at the La lattice site and U at the Hf lattice site is energetically most favorable. This behavior is consistent with the individual doped systems.

3.5. PL

Figure 4a shows the PL emission spectrum of LHO NPs under 305 nm. The emission spectra showed a broad band around 400 nm in violet blue region. We have used DFT calculations in our earlier work to probe the same and found the presence of doubly ionized oxygen vacancies (V_O^{2+}) is the most probable defect responsible for visible PL in LHO NPs.[6,9] The violet-blue emission in the LHO NPs is attributed to electronic transition from defect state located around 3.5 eV to valence band maxima (VBM). The recombination of photoexcited holes with electrons present in the OVs leads to violet blue emission in the LHO NPs. The excitation spectrum of the LHO NPs (λ_{em} = 400 nm) is shown in Figure 5a depicted a broad band peaking around 305 nm which was ascribed to the combined effect of electronic transitions involving defect states and $O^{2-} \rightarrow Hf^{4+}$ ion.

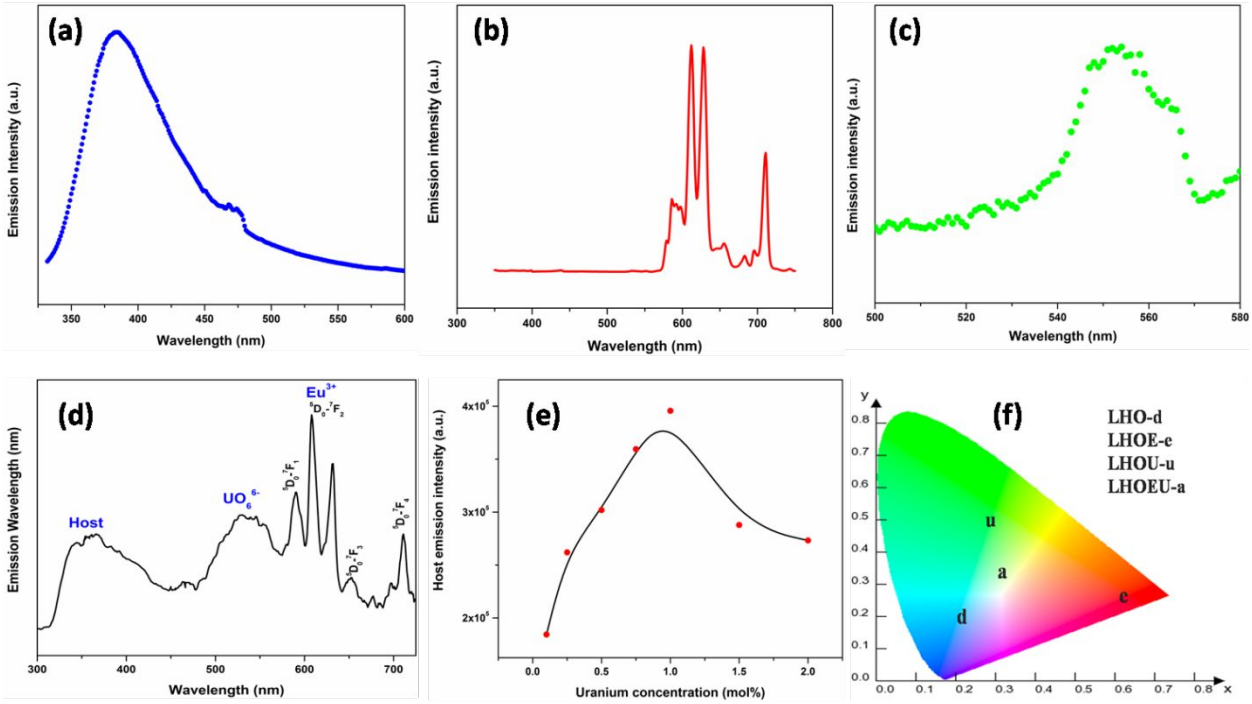

Figure 4. Emission spectra of the (a) LHO, (b) LHOE, (c) LHOU, and (d) LHOEU NPs under 305 nm excitation. (e) Effect of uranium doping concentration on PL emission intensity of the LHO host co-doped with Eu^{3+} in the wavelength range of 300-450 nm. (f) Color coordinate diagram showing light emitted from the LHO, LHOE, LHOU, and LHOEU NPs.

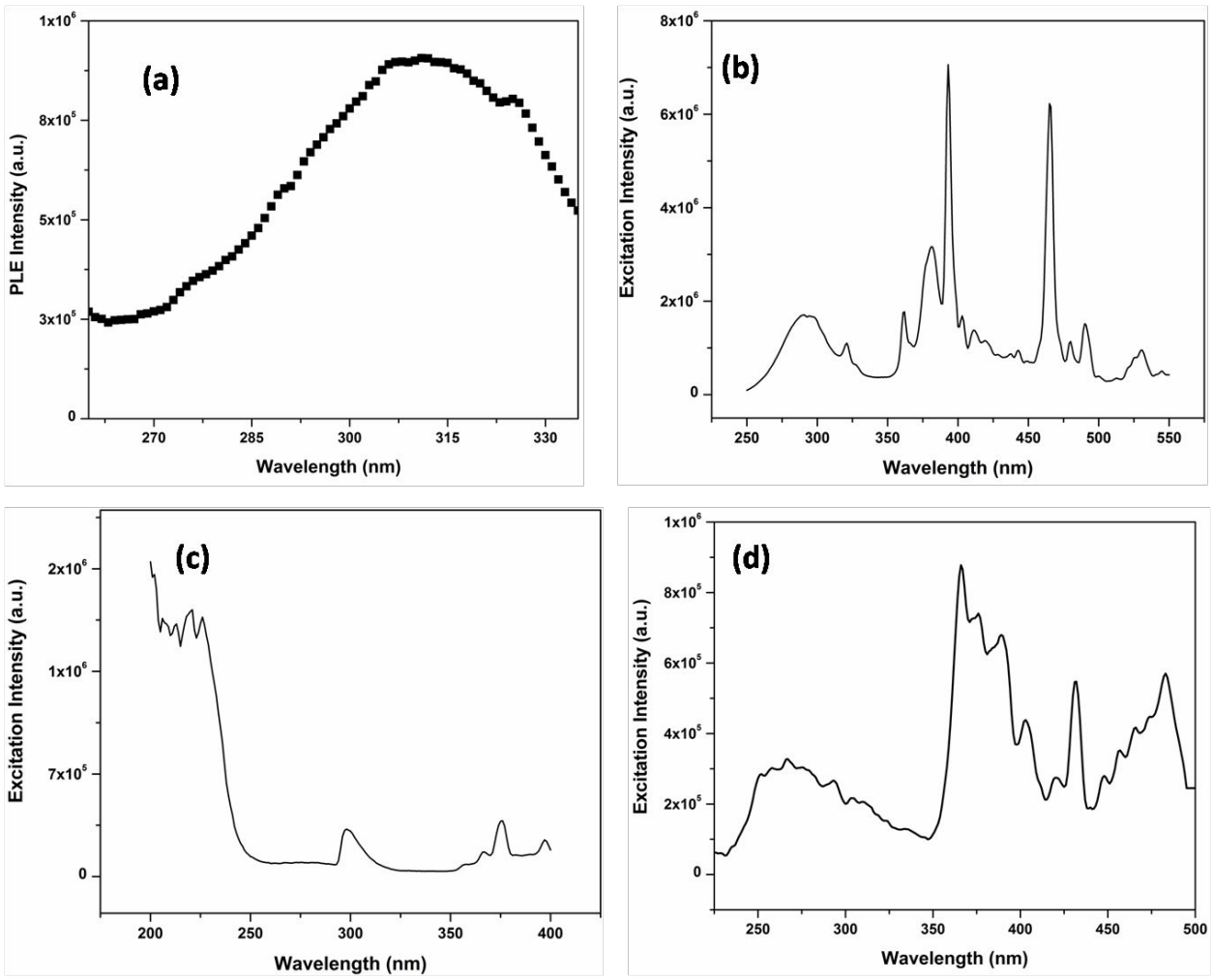

Figure 5. Excitation spectra of the (a) LHO (λ_{em} = 400 nm), (b) LHOE (λ_{em} = 616 nm), (c) LHOU (λ_{em} = 556 nm), and (d) LHOEU (λ_{em} = 616 nm) NPs.

Figure 4b shows the emission spectra of the LHOE NPs under 305 nm which displayed the typical Eu^{3+} features of $^5D_0 \rightarrow {}^7F_J$ (J = 1-4) transitions. The spectrum displayed an intense peak at 616 nm due to the hypersensitive electric dipole transition compared to the peak at 591 nm due to the magnetic dipole transition. This suggests low local symmetry around europium ion in the LHO host which is in line with our earlier report on the LHOE NPs.[6,9] Figure 5b shows the typical excitation spectra of the LHOE NPs consisting of broad $O^{2-} \rightarrow Eu^{3+}$ charge transfer band in the region of 200-300 nm and the fine intra-configuration f-f transition features of Eu^{3+} in the region of 350-550 nm.

Surface defects and cation vacancies are deleterious to PL as they provide non-radiative pathways and may quench the luminescence. However, oxygen vacancies lead to enhanced PL in case of

doped phosphors by acting as sensitizer and mediate HDET and the process is known as host sensitized energy transfer (HSET).[47] Wide band gap of LHO (~4.3 eV) may easily accommodate Eu^{3+} 4f energy levels which lead to strong interaction between O^{2-} 2p states and Eu^{3+} d/f states enabling efficient HDET.[48] In the LHOE NPs, energy transfer is induced through doubly ionized oxygen vacancies (V_O^{2+}) lying in the LHO band gap to Eu^{3+}excited levels. Eu^{3+} d/f states are present in both VB and CB minority and majority spin components in the LHO host.[9] The HSET mechanism is shown schematically in Figure S2. Based on the Dexter concept of energy transfer, efficient energy transfer can only happen when there is a spectral overlap between the donor emission and the acceptor excitation (LHO and Eu^{3+}ion, respectively, in this case).[49] To further validate these results, our experimental results with clear spectral overlap between the emission of the LHO host (donor) and excitation of Eu^{3+} ion (acceptor) (Figure 6a) suggested an efficient energy transfer from the host to the dopant ions. Figure 6b clearly showed complete disappearance of host emission in case of the LHOE NPs when compared with the emission spectrum of the LHO NPs while both the emission spectra were recorded under the identical conditions of excitation wavelength, slit width, and dwell time to avoid any discrepancies.

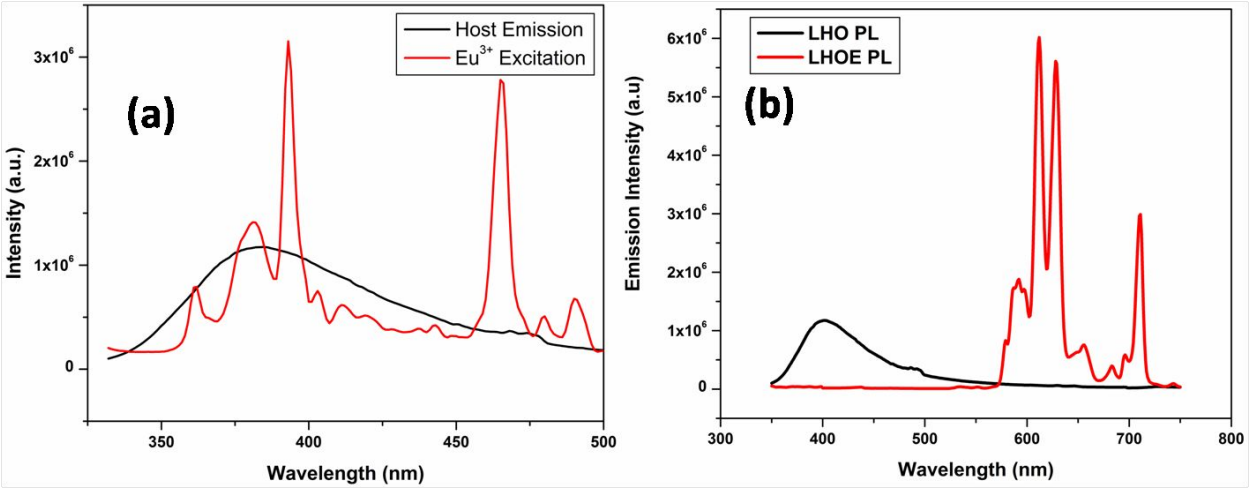

Figure 6. (a) The emission spectrum of the LHO NPs and the excitation spectrum of the LHOE NPs and (b) PL emission spectra of the LHO and LHOE NPs showing the energy transfer from the LHO host to Eu^{3+} ion in the LHOE NPs.

Figure 4c shows the emission spectra (λ_{ex} = 305 nm) of the LHOU NPs wherein a broad band peaking at 556 nm was observed which is typical of uranium in +6 oxidation state existing in the form of octahedral uranate (UO_6^{6-}) having U-O moiety.[5] It arises due to ligand to metal charge

transfer (LMCT) involving bonding oxygen (Π_u, Π_g, Ω_g, and Ω_u orbitals) to nonbonding uranium ($5f_\delta$ and $5f_\Phi$ orbitals). Figure 5c shows the excitation spectra (λ_{em} = 556 nm) of the LHOU NPs which displayed dual features of a shoulder spanning 200-250 nm ascribed to $O^{2-} \rightarrow U^{6+}$ charge transfer band and the fine features in the range of 300-400 nm because of the intra-configuration f-f bands of uranium ion.

Figure 4d shows the emission spectrum of the LHOEU NPs (1.0% Eu^{3+} and 1.0% U^{6+}) at 305 nm excitation. Here we found that the efficient HDET previously observed in case of the LHOE NPs was completely curtailed off. This emission spectrum was rich in all three components: defect induced blue emission, uranium induced green emission, and europium induced red emission. The efficacy of HDET was further confirmed by monitoring the PL emission of the LHOEU NPs with varying uranium doping concentrations from 0.1 to 2.0mol% (Figure 7a).

Upon uranium doping, it suppresses the formation of OVs but the europium PL can be seen from the LHOUE NPs. This is because the excitation at 305 nm can also directly excite europium ion through its intra-configurational f-f contribution of $^7F_0 \rightarrow {}^5H_6$ transition.[50] Proposed contrasting mechanisms of europium PL in the LHOE and LHOEU NPs are shown in Figure S3.

We have also calculated the color coordinates of the LHOEU NPs for different uranium concentrations (Figure S4). Clear color tunability from red to near white to white emission can be clearly seen. The digital camera image of the LHOE and LHOEU NPs (Figure S5) clearly show red and white emissions from the respective samples.

XRD patterns showed no impurity or any phase separation from the LHOEU NPs at different uranium concentrations (Figure 7b). All these LHOEU NPs were single phase samples matching with the LHO host having space group Fd-3m and ordered pyrochlore structure.

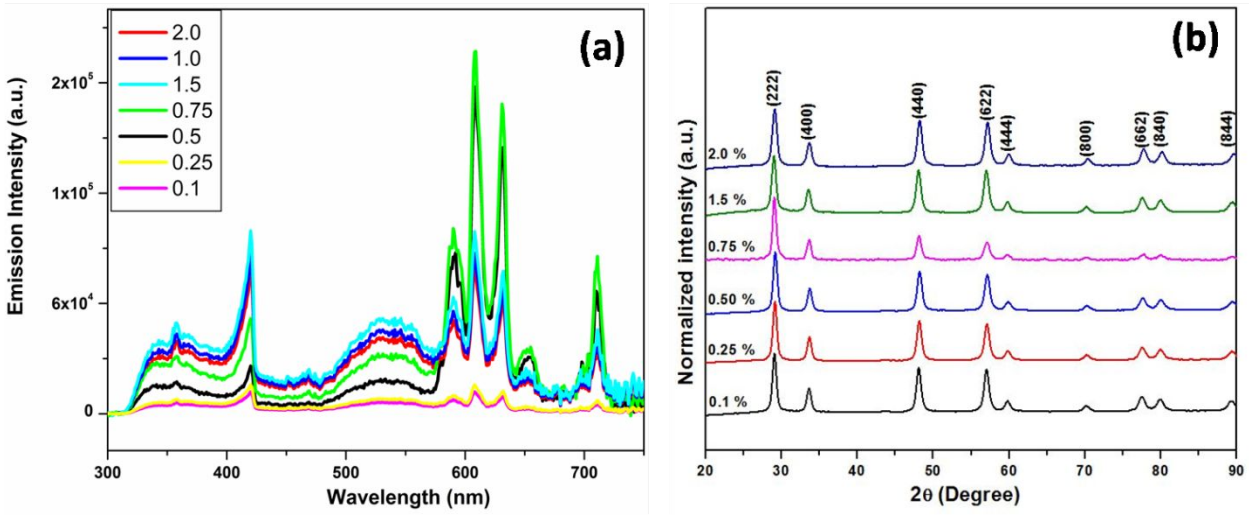

Figure 7. (a) Emission spectra of the LHOEU NPs with different uranium doping concentrations (0.1-2.0 mol%) under 305 nm excitation and (b) XRD patterns of the LHOEU (%U = 0.1, 0.25, 0.5, 0.75, 1.5, and 2.0) NPs.

It is clearly seen from Figure 7a that the host emission increased as the uranium concentration increased up to 1.0 mol %, and then reduced beyond 1.0% uranium doping concentration owing to the reduced density of oxygen vacancies. DFT calculated most stable local site of uranium in the LHO host suggested that uranium has high probability to stabilize at Hf^{4+} site compared to La^{3+} site whereas the reverse is true for europium ion. As more and more U^{6+} ion is co-doped inside the LHO lattice, there is a progressive increase in the density of hafnium vacancies and antisite defect (U@Hf) to invoke the need of charge compensation owing to aliovalent substitution of U^{6+} ion at Hf^{4+} site. Presence of negatively charged cation vacancies may annihilate the positively charge oxygen vacancies intrinsically present in pyrochlore structured LHO. This initial increase of the host emission with the increase of uranium concentration up to 1.0mol% can be ascribed to suppression of energy transfer from the LHO host to europium ion. This suppression of HDET by uranium can be ascribed to different mechanisms. Firstly, uranium ion acted as a barrier between the LHO host and dopant (Eu^{3+}) inside the LHOEU NPs to inhibit HDET. It is believed that co-doping uranium in the LHOE lattice enhanced the separation between defect sites and europium dopant which reduced the HDET and rather led to increase in violet blue emission due to an increase probability of radiative recombination of photoexcited holes and electrons in the valence band. The excitation spectrum of the LHOEU NPs (Figure 5d) also clearly showed the typical

features of defects, uranium and europium, which further suggested uranium acts as a barrier to increase the separation between defect and europium ion. In particular, several fine peaks in the region of 350-500 nm can be ascribed to the Eu^{3+} f–f transitions of $^7F_0 \rightarrow {}^5H_6$ (300 nm), $^7F_0 \rightarrow {}^5H_3$ (320 nm), $^7F_0 \rightarrow {}^5D_4$ (360 nm), $^7F_0 \rightarrow {}^5G_J$ (385 nm), $^7F_0 \rightarrow {}^5L_6$ (395 nm), $^7F_1 \rightarrow {}^5D_3$ (416 nm), and $^7F_0 \rightarrow {}^5D_2$ (464 nm).

Secondly, charge neutralization requires occupancy of $3Hf^{4+}$ sites by $2U^{6+}$ ions leading to the formation of cation vacancy V''''_{Hf} and antisite defect $U^{\cdot\cdot\cdot\cdot}_{Hf}$. These defects absorb the photons emitted by the LHO host and back transfer to the host itself. This back transferred energy to europium ion enhanced the LHO host emission itself. Phosphorus ion is also reported to minimize non-radiative energy transfer between vanadate host and Dy^{3+} ion.[26]

Color coordinated diagram of the LHO, LHOE, LHOU and LHOEU NPs is shown in Figure 4f. The violet blue (marked as letter *d*), red (marked as letter *e*), and green (marked as letter *u*) light emissions can be clearly seen from the LHO, LHOE, and LHOU NPs, respectively. The interesting part is the color coordinates of the LHOEU NPs indicated the color domain close to 0.312 and 0.323 giving almost perfect white light (Figure 4findicatedby letter *a*). It was owing to the combined emissions from the blue, green and red hues. The quantum yield (QY) of the LHOE NPs has been previously reported as ~16.5 %.[8] whereas the QY of the LHOEU NPs depicting white light emission calculated in this work was found to be approximately 12.4%. Compared to commercial white phosphors, it is low and further improvement is necessary. Considering the potential of tuning the color coordinates by actinide doping and the efficacy of LHO as luminescence host, we will explore several other strategies to improve the QY in our future work. These strategies could include quenching surface defects by core-shell strategy, annealing out charge compensating defects, co-doping by alkali ions, and co-precipitating pH and optimizing the ideal thermal conditions in MSS. In our previous work on $La_2Hf_2O_7:Eu^{3+}$[9] and $La_2Hf_2O_7:Sm^{3+}$[7], we have carried out in situ PL measurements and found that the activation energies for thermal quenching were 0.41 eV and 0.153 eV, respectively, highlighting the potential of LHO as a luminescent host. Particularly, the thermal stability of the $La_2Hf_2O_7:Eu^{3+}$ NPs was quite good with 54% intensity retained up till 700 K.

4. DFT calculations

4.1. Electronic structure of LHOE

To investigate the effect of Eu doping on the electronic structure of $La_2Hf_2O_7$, we have calculated DOS for both types of Eu defects, i.e., substitution of one La or Hf site by an Eu ion (Eu_{La} and Eu_{Hf}, respectively). Figures 8a and 8b show the DOS plots for $La_2Hf_2O_7$ with the Eu_{La} and Eu_{Hf} defects, respectively. The electronic structure for the both defect types of Eu-doped $La_2Hf_2O_7$ system looks very much similar to that of undoped system. However, Eu(p) and Eu(d) orbitals contribute to both VBM and CBM, leading to very small changes in energy levels of the band edges with respect to that of ideal $La_2Hf_2O_7$ while Eu(d) states spread throughout the VB and CB.

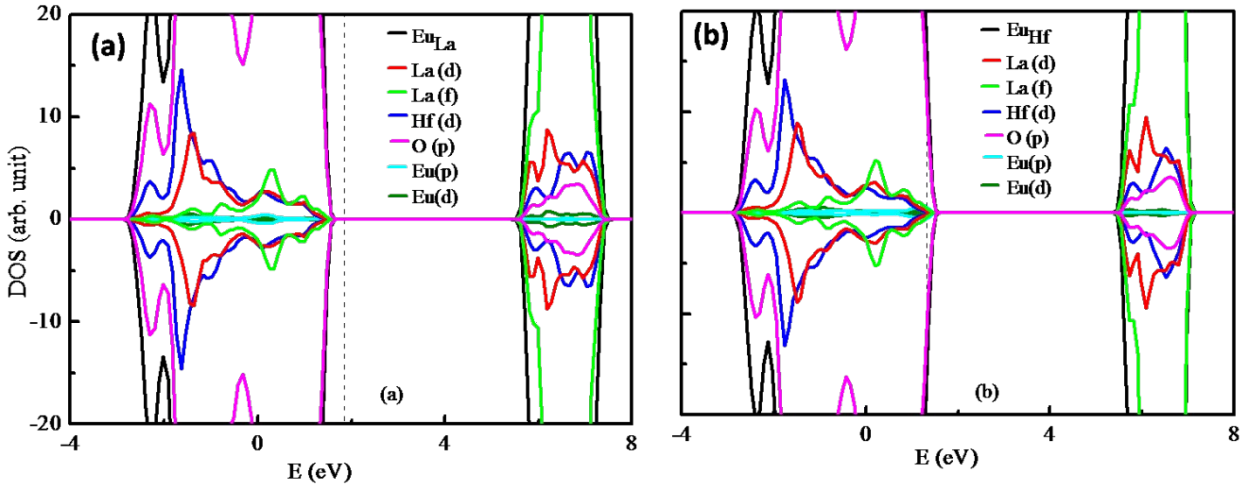

Figure 8. Density of states of the (a) Eu_{La} and (b) Eu_{Hf} defects in the LHO host. Vertical dashed line indicates Fermi level.

4.2. Electronic structure of LHOU

To investigate the effect of U doping on the electronic structure of $La_2Hf_2O_7$, we have calculated DOS for both the types of U defects. Figure 9a shows the DOS plot for U-doped $La_2Hf_2O_7$ with U at La site (U_{La}) while Figure 9b shows the DOS plot for U-doped $La_2Hf_2O_7$ with U at Hf site (U_{Hf}). As can be seen from Figure 9a, when U substitutes the La site, it introduces shallow defect states just below the CBM by an energy level of 0.55 eV. The defects states are found to be partially occupied in nature. This may be due to the presence of excess electron in the system. Analysis of PDOS shows that the shallow defect states are mainly composed of U(f) orbitals with minor contribution of U(d) and O(p) orbitals. In contrastingly, U doping at the Hf lattice site introduces fully occupied impurity states close to the CBM (0.56 eV) (Figure 9b). These states are contributed mainly by U(f) orbitals with minor contribution of La(d), La(f), and O(p) orbitals.

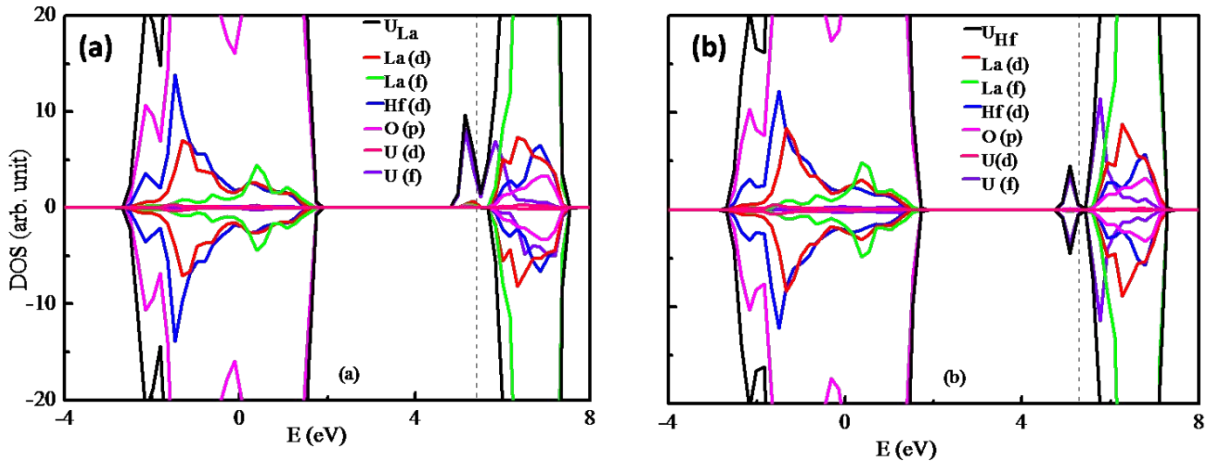

Figure 9. Density of states of (a) U_{La} and (b) U_{Hf} defects in the LHO host. Vertical dashed line indicates Fermi level.

4.3. Electronic structure of (Eu, U) co-doped $La_2Hf_2O_7$

To investigate the effect of co-doping with U into Eu-doped $La_2Hf_2O_7$, we have calculated DOS for the four different configurations, i.e., (Eu_{La} + U_{La}), (Eu_{Hf} + U_{Hf}), (Eu_{La} + U_{Hf}), and (U_{La} + La_{Hf}) (Figure 10). The DOS plot for $La_2Hf_2O_7$ in the presence of Eu and U at the La lattice site as Eu_{La} + U_{La} defects indicates that there exist partially occupied shallow impurity states at 0.70 eV below the CBM (Figure 10a). The impurity states are composed of U(f) orbitals. The VBM and CBM levels are found to be lifted by 0.25 eV and 0.19 eV, respectively. Fermi level is shifted towards the CBM because of excess electron in the system. The DOS plot for $La_2Hf_2O_7$ in the presence of Eu and U at the Hf lattice sites as Eu_{Hf} + U_{Hf} defects shows that there is partially occupied impurity state (spin-down direction) at 1.7 eV below the CBM (Figure 10b). The partially unoccupied impurity states are observed in the forbidden region at 0.21 eV and 0.63 eV below the CBM. The impurity states are composed of mainly U(f) orbitals. The VBM and CBM levels are shifted by 0.18 eV (upward) and 0.14 eV (downward), respectively. Figure10cshows the DOS plot for $La_2Hf_2O_7$ in the presence of Eu and U at the La and Hf lattice sites as Eu_{La} + U_{Hf} defects, respectively. In this case, the discrete occupied impurity states are observed at 0.58eV below the CBM. The occupied impurity states are composed of mainly U(f) orbital with minor contribution O(p) and La(d) orbitals. The VBM and CBM are increased by 0.15 eV and 0.09 eV with respect to defect free $La_2Hf_2O_7$, respectively. Figure 10d shows the DOS plot for $La_2Hf_2O_7$ in the presence of Eu and U at the Hf and La lattice sites as U_{La} + La_{Hf} defects, respectively. In this case, partially

occupied and unoccupied impurity states are observed at 1.18 eV and 0.57 eV below the CBM, respectively. The occupied impurity states are composed of mainly U(f) orbital with minor contribution O(p) and La(f) orbitals. The VBM is shifted by 0.31 eV (upward) and the CBM is shifted by 0.3 eV (downward) with respect to defect free $La_2Hf_2O_7$, respectively.

Previous study indicated that monodoping with Eu is accompanied by oxygen vacancy defects, which creates discrete mid-gap states resulting in the significant change in the emission behavior of $La_2Hf_2O_7$ facilitated by the host to europium energy transfer.[9] However, co-doping U into Eu-doped $La_2Hf_2O_7$ makes the system electron rich. Thus, formation of cation vacancy is expected to compensate the excess charge in the co-doped system. This indirectly indicates that the formation of oxygen vacancy is suppressed due to co-doping U into Eu-doped $La_2Hf_2O_7$. In general, the role of anion vacancy defects is much more prominent on the optical properties over cation vacancy. This is one of factors influencing the change of observed optical behavior of our Eu-doped $La_2Hf_2O_7$ NPs due to co-doping with U resulting in the inhibition of host to europium energy transfer.

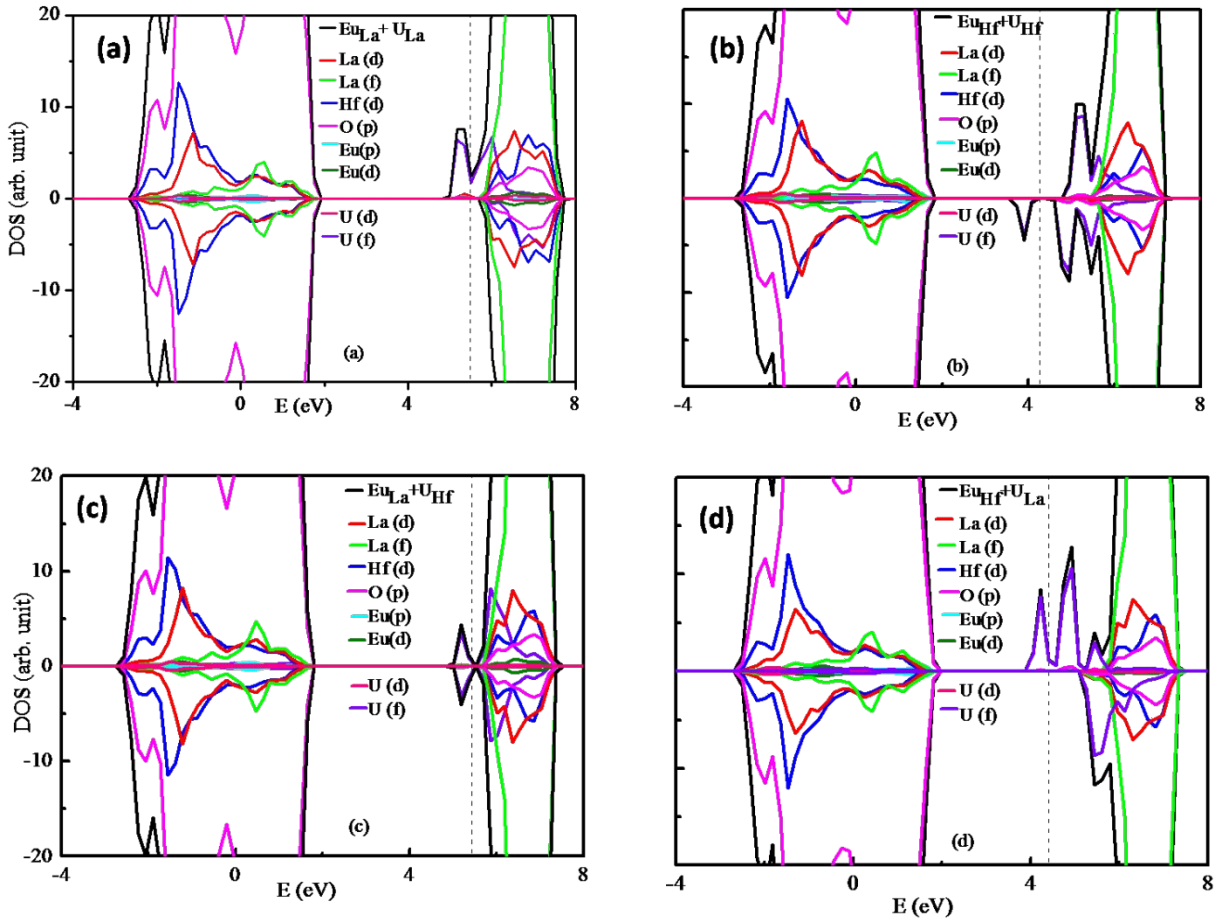

Figure 10. Density of states of (a) Eu_{La} + U_{La}, (b) Eu_{Hf} + U_{Hf}, (c) Eu_{La} + U_{Hf}, and (d) U_{La} + La_{Hf} defects in the LHO host. Vertical dashed line indicates Fermi level.

Conclusions

In summary, we synthesized $La_2Hf_2O_7$, $La_2Hf_2O_7$:Eu^{3+}, $La_2Hf_2O_7$:U^{6+}, and $La_2Hf_2O_7$:Eu^{3+},U^{6+} NPs using a molten salt synthesis method in the work. All these NPs stabilized in an ideal pyrochlore structure with ellipsoidal morphology though uranium co-doping led to enhanced HfO_6 distortion. The undoped LHO NPs displayed defect induced violet blue emission which can be tuned to red and green emission by doping europium and uranium, respectively. Here, for the first time, we adopted a novel design strategy to utilizing the emission coming from the host, dopant and co-dopant by restricting host to dopant energy transfer as demonstrated by uranium co-doping into the $La_2Hf_2O_7$:Eu^{3+} NPs which completely suppressed the HDET by acting as a barrier to enhance the separation between defect and europium ion. Furthermore, it was found that with increased uranium concentration, the intensity of host emission increased as triggered by absorption of host emission by the lanthanum and hafnium vacancies and back transfer to host. Based on DFT calculations, it was found that europium stabilized at La^{3+} site whereas uranium prefers Hf^{4+} site making the co-doped system highly electron rich owing to the formation of negatively charged lanthanum and hafnium vacancies. Formation of cation vacancy is expected to compensate the excess charge in the co-doped system while suppressing the formation of oxygen vacancy due to co-doping of U into the Eu-doped $La_2Hf_2O_7$ NPs. Furthermore, the color of emission can also be tuned from blue to green to red by moving from undoped LHO NPs, to europium doped LHO NPs, and to uranium and europium co-doped LHO NPs. Interestingly, white light emission was observed by co-doping Eu^{3+} (1.0mol%) and U^{6+} (1.0mol%) in the LHOEU NPs.

Acknowledgement

YM would like to thank the support by the National Science Foundation under CHE (award #1952803 and #1710160) and the IIT startup funds. SKG thanks the United States-India Education Foundation (USIEF) and the Institute of International Education (IIE) for his Fulbright Nehru Postdoctoral Fellowship (Award#2268/FNPDR/2017). We also appreciate Jose P. Zuniga and Maya Abdou for assistance on sample synthesis.

References:

[1] Y.N. Ahn, K. Do Kim, G. Anoop, G.S. Kim, J.S. Yoo, Design of highly efficient phosphor-converted white light-emitting diodes with color rendering indices (R 1− R 15)≥ 95 for artificial lighting, Scientific reports 9 (2019) 1-10.

[2] J.-S. Li, Y. Tang, Z.-T. Li, J.-X. Li, X.-R. Ding, B.-H. Yu, S.-D. Yu, J.-Z. Ou, H.-C. Kuo, Toward 200 Lumens per Watt of Quantum-Dot White-Light-Emitting Diodes by Reducing Reabsorption Loss, ACS Nano (2020).

[3] S.K. Gupta, J.P. Zuniga, M. Abdou, M.P. Thomas, M.D.A. Goonatilleke, B.S. Guiton, Y. Mao, Lanthanide-doped lanthanum hafnate nanoparticles as multicolor phosphors for warm white lighting and scintillators, Chemical Engineering Journal 379 (2020) 122314.

[4] S.K. Gupta, V. Grover, R. Shukla, K. Srinivasu, V. Natarajan, A.K. Tyagi, Exploring pure and RE co-doped (Eu^{3+}, Tb^{3+} and Dy^{3+}) gadolinium scandate: Luminescence behaviour and dynamics of energy transfer, Chemical Engineering Journal 283 (2016) 114-126.

[5] M. Abdou, S.K. Gupta, J.P. Zuniga, Y. Mao, On structure and phase transformation of uranium doped $La_2Hf_2O_7$ nanoparticles as an efficient nuclear waste host, Materials Chemistry Frontiers 2 (2018) 2201-2211.

[6] S.K. Gupta, M. Abdou, P.S. Ghosh, J.P. Zuniga, E. Manoharan, H. Kim, Y. Mao, On comparison of luminescence properties of $La_2Zr_2O_7$ and $La_2Hf_2O_7$ nanoparticles, Journal of the American Ceramic Society 103 (2020) 235-248.

[7] S.K. Gupta, M. Abdou, J.P. Zuniga, A.A. Puretzky, Y. Mao, Samarium-Activated $La_2Hf_2O_7$ Nanoparticles as Multifunctional Phosphors, ACS Omega 4 (2019) 17956-17966.

[8] S.K. Gupta, J.P. Zuniga, M. Abdou, Y. Mao, Thermal annealing effects on $La_2Hf_2O_7$:Eu^{3+} nanoparticles: a curious case study of structural evolution and site-specific photo- and radio-luminescence, Inorganic Chemistry Frontiers 5 (2018) 2508-2521.

[9] S.K. Gupta, J.P. Zuniga, P.S. Ghosh, M. Abdou, Y. Mao, Correlating Structure and Luminescence Properties of Undoped and Eu^{3+}-Doped $La_2Hf_2O_7$ Nanoparticles Prepared with Different Coprecipitating pH Values through Experimental and Theoretical Studies, Inorganic Chemistry 57 (2018) 11815-11830.

[10] Y. Ji, D. Jiang, J. Shi, $La_2Hf_2O_7$:Ti^{4+} ceramic scintillator for x-ray imaging, Journal of Materials Research 20 (2005) 567-570.

[11] Y.M. Ji, D.Y. Jiang, Y.K. Liao, J.L. Shi, Fabrication and Spectroscopic Investigation of $La_2Hf_2O_7$-Based Phosphors, Key Engineering Materials 280-283 (2004) 577-580.

[12] Y.-m. Ji, D.-y. Jiang, J.-l. Shi, Preparation and spectroscopic properties of $La_2Hf_2O_7$/Tb, Materials Letters 59 (2005) 868-871.

[13] J. Trojan-Piegza, S. Gierlotka, E. Zych, W. Lojkowski, Spectroscopic Studies of Nanopowder and Nanoceramics $La_2Hf_2O_7$:Pr Scintillator, Journal of the American Ceramic Society 97 (2014) 1595-1601.

[14] J. Trojan-Piegza, E. Zych, White persistent luminescence of $La_2Hf_2O_7$:Ti,Pr, Optical Materials 113 (2021) 110896.

[15] J. Trojan-Piegza, E. Zych, M. Kosińska, Fabrication and spectroscopic properties of nanocrystalline $La_2Hf_2O_7$:Pr, Radiation Measurements 45 (2010) 432-434.

[16] J. Zhang, K. Tse, M. Wong, Y. Zhang, J. Zhu, A brief review of co-doping, Frontiers of Physics 11 (2016) 117405.

[17] W. Luo, R. Li, X. Chen, Host-Sensitized Luminescence of Nd^{3+} and Sm^{3+} Ions Incorporated in Anatase Titania Nanocrystals, The Journal of Physical Chemistry C 113 (2009) 8772-8777.

[18] S.K. Gupta, R. Kadam, P. Pujari, Lanthanide spectroscopy in probing structure-property correlation in multi-site photoluminescent phosphors, Coordination Chemistry Reviews 420 (2020) 213405.

[19] A. Biswas, R. Bakthavatsalam, J. Kundu, Efficient Exciton to Dopant Energy Transfer in Mn^{2+}-Doped $(C_4H_9NH_3)_2PbBr_4$ Two-Dimensional (2D) Layered Perovskites, Chemistry of Materials 29 (2017) 7816-7825.

[20] J. Llanos, D. Espinoza, R. Castillo, Energy transfer in single phase Eu^{3+}-doped Y_2WO_6 phosphors, RSC Advances 7 (2017) 14974-14980.

[21] Z. Xianju, Y. Xiaodong, X. Tengjiao, Z. Kaining, C. Tianyu, Y. Hao, W. Zhongqing, Luminescence properties and energy transfer of host sensitized $CaMoO_4$:Tb^{3+} green phosphors, Journal of Rare Earths 31 (2013) 655-659.

[22] S.K. Gupta, P.S. Ghosh, N. Pathak, A. Arya, V. Natarajan, Understanding the local environment of Sm^{3+} in doped $SrZrO_3$ and energy transfer mechanism using time-resolved luminescence: a combined theoretical and experimental approach, RSC Advances 4 (2014) 29202-29215.

[23] S.K. Gupta, P.S. Ghosh, A.K. Yadav, S.N. Jha, D. Bhattacharyya, R.M. Kadam, Origin of Blue-Green Emission in α-$Zn_2P_2O_7$ and Local Structure of Ln^{3+} Ion in α-$Zn_2P_2O_7$:Ln^{3+} (Ln = Sm, Eu): Time-Resolved Photoluminescence, EXAFS, and DFT Measurements, Inorganic Chemistry 56 (2017) 167-178.

[24] S.K. Gupta, P.S. Ghosh, A.K. Yadav, N. Pathak, A. Arya, S.N. Jha, D. Bhattacharyya, R.M. Kadam, Luminescence Properties of $SrZrO_3$/Tb^{3+} Perovskite: Host-Dopant Energy-Transfer Dynamics and Local Structure of Tb^{3+}, Inorganic Chemistry 55 (2016) 1728-1740.

[25] S.K. Gupta, M. Sahu, P.S. Ghosh, D. Tyagi, M.K. Saxena, R.M. Kadam, Energy transfer dynamics and luminescence properties of Eu^{3+} in $CaMoO_4$ and $SrMoO_4$, Dalton Transactions 44 (2015) 18957-18969.

[26] N.S. Singh, N.K. Sahu, D. Bahadur, Multicolor tuning and white light emission from lanthanide doped $YPVO_4$ nanorods: energy transfer studies, Journal of Materials Chemistry C 2 (2014) 548-555.

[27] W. Lee, J.W. Han, Y. Chen, Z. Cai, B. Yildiz, Cation Size Mismatch and Charge Interactions Drive Dopant Segregation at the Surfaces of Manganite Perovskites, Journal of the American Chemical Society 135 (2013) 7909-7925.

[28] L. Lv, T. Wang, S. Li, Y. Su, X. Wang, Tuning the optical, electronic and luminescence properties of LaOCl:Eu^{3+} via structural and lattice strain modulation, CrystEngComm 18 (2016) 907-916.

[29] W.J. Chung, J.Y. Lee, The role of the bulky blocking unit of the fluorescent emitter in efficient green hyper-fluorescent organic light-emitting diodes, Journal of Information Display (2020) 1-6.

[30] F. Kang, L. Li, J. Han, D.Y. Lei, M. Peng, Emission color tuning through manipulating the energy transfer from $VO4^{3-}$ to Eu^{3+} in single-phased $LuVO_4$:Eu^{3+} phosphors, Journal of Materials Chemistry C 5 (2017) 390-398.

[31] M. Kumar, M. Mohapatra, A case study of energy transfer mechanism from uranium to europium in $ZnAl_2O_4$ spinel host by photoluminescence spectroscopy, Spectrochimica Acta Part A: Molecular and Biomolecular Spectroscopy 159 (2016) 42-47.

[32] P.E. Blöchl, Projector augmented-wave method, Physical review B 50 (1994) 17953.

[33] G. Kresse, D. Joubert, From ultrasoft pseudopotentials to the projector augmented-wave method, Physical review B 59 (1999) 1758.

[34] J.P. Perdew, K. Burke, M. Ernzerhof, Generalized gradient approximation made simple, Physical review letters 77 (1996) 3865.

[35] J.P. Perdew, J.A. Chevary, S.H. Vosko, K.A. Jackson, M.R. Pederson, D.J. Singh, C. Fiolhais, Atoms, molecules, solids, and surfaces: Applications of the generalized gradient approximation for exchange and correlation, Physical review B 46 (1992) 6671.

[36] H.J. Monkhorst, J.D. Pack, Special points for Brillouin-zone integrations, Physical review B 13 (1976) 5188.

[37] M. Subramanian, G. Aravamudan, G.S. Rao, Oxide pyrochlores—a review, Prog.Solid Sate Chem. 15 (1983) 55-143.

[38] F.N. Sayed, V. Grover, K. Bhattacharyya, D. Jain, A. Arya, C. Pillai, A. Tyagi, $Sm_{2-x}Dy_xZr_2O_7$ pyrochlores: probing order− disorder dynamics and multifunctionality, Inorg. Chem. 50 (2011) 2354-2365.

[39] K.M. Turner, D.R. Rittman, R.A. Heymach, C.L. Tracy, M.L. Turner, A.F. Fuentes, W.L. Mao, R.C. Ewing, Pressure-induced structural modifications of rare-earth hafnate pyrochlore, J. Phys.: Condens. Matter 29 (2017) 255401.

[40] J.P. Zuniga, S.K. Gupta, M. Abdou, Y. Mao, Effect of molten salt synthesis processing duration on the photo- and radioluminescence of UV-, Visible-, and X-ray-excitable $La_2Hf_2O_7:Eu^{3+}$ nanoparticles, ACS Omega 3 (2018) 7757-7770.

[41] M. Pokhrel, S.K. Gupta, K. Wahid, Y. Mao, Pyrochlore Rare-Earth Hafnate $RE_2Hf_2O_7$ (RE = La and Pr) Nanoparticles Stabilized by Molten-Salt Synthesis at Low Temperature, Inorganic Chemistry (2019).

[42] N. Garg, K.K. Pandey, C. Murli, K.V. Shanavas, B.P. Mandal, A.K. Tyagi, S.M. Sharma, Decomposition of lanthanum hafnate at high pressures, Phys. Rev. B 77 (2008) 214105.

[43] A. Slifka, B. Filla, J. Phelps, G. Bancke, C. Berndt, Thermal conductivity of a zirconia thermal barrier coating, Journal of Thermal Spray Technology 7 (1998) 43-46.

[44] H. Yamamura, H. Nishino, K. Kakinuma, K. Nomura, Electrical conductivity anomaly around fluorite–pyrochlore phase boundary, Solid State Ionics 158 (2003) 359-365.

[45] P. Modak, B. Modak, Insight into enhanced thermoluminescence property of (Mg, Cu, Ag)-Doped LiF: A DFT study, Journal of Luminescence 231 117779.

[46] P. Modak, B. Modak, Exploring the role of vacancy defects in the optical properties of LiMgPO 4, Physical Chemistry Chemical Physics 22 (2020) 16244-16257.

[47] S.K. Gupta, K. Sudarshan, P.S. Ghosh, A.P. Srivastava, S. Bevara, P.K. Pujari, R.M. Kadam, Role of various defects in the photoluminescence characteristics of nanocrystalline $Nd_2Zr_2O_7$: an investigation through spectroscopic and DFT calculations, Journal of Materials Chemistry C 4 (2016) 4988-5000.

[48] X. Qin, X. Liu, W. Huang, M. Bettinelli, X. Liu, Lanthanide-Activated Phosphors Based on 4f-5d Optical Transitions: Theoretical and Experimental Aspects, Chemical Reviews 117 (2017) 4488-4527.

[49] D.L. Dexter, A Theory of Sensitized Luminescence in Solids, The Journal of Chemical Physics 21 (1953) 836-850.

[50] S.A. Vieira, N. Rakov, C.B. de Araújo, E.L. Falcão-Filho, Upconversion luminescence in europium doped Y_2O_3 powder excited by absorption of three, four, and five infrared photons, Optical Materials Express 9 (2019) 3952-3961.